Mechanical vibration of a cylindrically rolled-up cantilever shell in microelectromechanical and nanoelectromechanical systems

W. Izumida,[1,*] Y. Hirayama,[1,2] H. Okamoto,[3] H. Yamaguchi,[1,3] and K.-J. Friedland[4]

[1]*Department of Physics, Tohoku University, Sendai 980-8578, Japan*

[2]*ERATO Nuclear Spin Electronics Project, Sendai 980-8578, Japan*

[3]*NTT Basic Research Laboratories, NTT Corporation, 3-1 Morinosato-Wakamiya, Atsugi 243-0198, Japan*

[4]*Paul-Drude-Institut für Festkörperelektronik, Hausvogteiplatz 5-7, D-10117 Berlin, Germany*

(Received 14 August 2011; revised manuscript received 21 December 2011; published 14 February 2012)

The mechanical vibration of a cylindrically rolled-up cantilever shell is studied for possible use as micro- and nano-electromechanical systems. The system is modeled as an isotropic open circular cylindrical shell of rectangular planform that is clamped along one straight edge and is free on the other three edges. The mechanical vibration is calculated using both numerical and analytical methods. The frequencies of the axial wave modes strongly increase when the curvature of the shell increases because the curvature induces in-plane extension. The frequencies of the bending in the circumference direction and twisting modes show weaker curvature dependence. Frequencies as a function of the curvature for the axial wave modes obey a scaling law different from that for the bending and twisting modes. Several possible electromechanical coupling mechanisms in micro- and nano-electromechanical systems are considered.

DOI: 10.1103/PhysRevB.85.075313 PACS number(s): 62.25.Jk, 63.22.−m, 68.60.Bs

I. INTRODUCTION

Microfabricated freestanding semiconductor structures have been investigated for use as micro- and nano-electromechanical systems (MEMS and NEMS).[1–10] Free electrons embedded in semiconductors, such as a high-mobility two-dimensional electron gas (2DEG), couple to the mechanical motion of the freestanding structure. This electromechanical coupling enables freestanding semiconductors to be used as force and displacement sensors based on transport measurements[2,3] and also to be used as tools for measuring semiconductor electronic properties such as a magnetization.[4–6] The dynamic back-action induced by the electron motion has been investigated because it enables not only the frequency and amplitude of the vibration modes to be changed but also the mechanical vibration to be dynamically amplified or cooled to enable the quantum mechanical behavior of mechanical systems to be studied.[7–10]

At the same time, the self-rolling of thin pseudomorphically strained semiconductor bilayer systems based on epitaxial heterojunctions grown by molecular-beam epitaxy have been proposed by Prinz and co-workers.[11,12] The optics in microtube ring resonators[13,14] and the transport of electrons on cylindrical surfaces[15–18] represent remarkable demonstrations of the new physical properties on curved surfaces. The rolled-up semiconductors, as well as nanocarbon materials of carbon nanotubes,[19] folded graphene,[20,21] and carbon nanoscrolls,[22,23] enable investigation of fundamental physical properties in a nontrivial geometry on curved surfaces.

Rolled-up structures are advantageous for sensitive mechanical sensors[24] because the curvature hardens the system. Moreover, rolled-up semiconductors containing 2DEG[15–18] are promising as new types of MEMS and NEMS. However, their mechanical vibration might create noise in the electron systems. Furthermore, the electrons could be a vibration damping source.[25] To control the vibrational and electronic properties and to avoid unfavorable effects such as a noise, it is important to understand the quantitative properties of mechanical vibration and electromechanical coupling mechanisms.

Mechanical vibration of curved plates, called shells, has been of interest mainly in the mechanical engineering research field for a long time. The vibrational properties of shells are much more complicated than those of flat plates because the curvature of shells generally induces coupling between the in-plane and out-of-plane modes. The curvature enters into the vibration problem not only by means of more complex equations of motion but through the boundary conditions as well. A huge number of articles on shell vibration have been published. An excellent summary of the work on shell vibration was presented in a monograph[26] by Leissa in 1973. Research developments related to shell vibration can be found in several review articles.[27–31] Circular cylindrical shells have been of particular interest in many studies. Many studies focused on the closed structures, i.e., the hollow tubes. For instance, most of Leissa's monograph[26] is devoted to closed circular cylindrical shells. There are many combinations of boundary conditions for an *open* circular cylindrical shell of rectangular planform, and each combination creates a distinct problem. There is no exact solution except for the case in which all edges are simply supported. In this case the displacements are represented by simple sinusoidal functions. The calculation of the mechanical vibration for each boundary condition of engineering interest has mainly been performed using numerical calculation.

Surprisingly, there has been little work on the mechanical vibration of an open circular cylindrical shell of rectangular planform that is clamped along one straight edge and free on the other three edges.[32–34] That is the structure focused on in the present paper. Although bending and twisting modes in the circumference direction have been shown to have little

curvature dependence, modes involving waves in the axis direction show a considerable frequency increase when curvature is induced.[32] However, the numerical calculations have been done for very limited parameter cases.[32–34] Therefore, we are still far from a quantitative and comprehensive understanding of the mechanical vibration of a cantilevered open circular cylindrical shell of rectangular planform. That is, there is still limited knowledge about the functional form of the frequency for various parameters.

In this paper we report on our theoretical study of the vibrational properties of a cylindrically rolled-up cantilever shell. We focus on the effects of the curvature on mechanical vibration. Several electromechanical coupling effects are also discussed.

The rolled-up structure is modeled as an isotropic one-straight-edge-clamped open circular cylindrical shell using Flügge shell theory. The mechanical vibrations are calculated numerically by the Rayleigh-Ritz method. Analytical calculations with perturbation analysis and simplified effective one-dimensional equations of motion are also performed as complementary methods. Modes involving waves in the cylinder axis direction, called here axial wave modes, have higher frequencies when the curvature of the structure is larger because the curvature induces in-plane extension. In contrast, bending in the circumference direction and twisting modes have weaker curvature dependence because of inextension. The axial wave modes obey a scaling law different from that of the bending and twisting modes. The theoretical study of vibrational properties described in this paper is applicable not only to micro- and nanomechanics but also to macroscale isotropic one-straight-edge-clamped open circular cylindrical shells. Capacitive coupling, deformation potential, and magnetically induced coupling are briefly discussed for the electromechanical coupling effects.

This paper is organized as follows. In Sec. II, the system is formulated. In Sec. III, numerical results are shown as a function of the curvature. To enable the curvature effects to be better understood, analytical results are presented. In Sec. IV, possible electromechanical coupling mechanisms are briefly discussed. Discussion of experiments and summary of the key points are given in Sec. V. Explanations of the derivation of strain energy, the boundary conditions of the system, and the perturbation analysis are given in Appendices A–C, respectively.

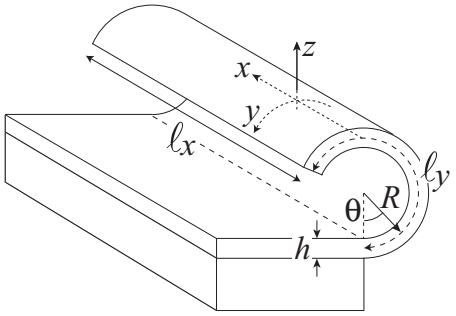

FIG. 1. Model of cantilevered circular cylindrical shell of rectangular planform. Cylindrical coordinates are denoted by (x,θ,z), and surface coordinates at middle surface are denoted by (x,y,z). The x axis is in the axis direction, the y axis is in the circumference direction, and the z axis is in the direction normal to the cylinder surface.

II. STRAIN ENERGY AND EQUATION OF MOTION

In this section we show the strain energy and the equation of motion for our system using Flügge shell theory. The formulation is well described elsewhere, e.g., in Leissa's monograph.[26] Explanations of the formulation for the strain energy and the boundary conditions are given in Appendices A and B, respectively.

The rolled-up structure is modeled as a one-side clamped open circular cylindrical shell with constant thickness h. The structure is made by rolling up a rectangular cantilevered plate. The geometry of the system is schematically shown in Fig. 1. Here we introduce cylindrical coordinates (x,θ,z). The x axis is in the cylinder axis direction, θ is the angle in the circumference direction, and the z axis is in the direction normal to the cylinder surface. The origin of the z coordinate is the middle surface of the shell. The radius of curvature at the middle surface is R. The length along the x direction is ℓ_x, and the arc length of the middle surface along the θ direction is ℓ_y. The clamped end is located at $\theta = 0$ along the x axis, the three free boundaries are located at $x = \pm\ell_x/2$, and $\theta = \ell_y/R$. We also introduce coordinate $y = R\theta$ on the middle surface.

Using the theory of thin shells for small displacement and the Kirchhoff-Love approximation, we write the strain energy with displacements u, v, and w in the x, y, and z directions, respectively, at the middle surface as

$$U = \frac{1}{2}\int dxdy \left\{ C\left[\left(\frac{\partial u}{\partial x}\right)^2 + \left(\frac{\partial v}{\partial y} + \frac{w}{R}\right)^2 + 2\nu\frac{\partial u}{\partial x}\left(\frac{\partial v}{\partial y} + \frac{w}{R}\right)\right] + \frac{1-\nu}{2}C\left(\frac{\partial u}{\partial y} + \frac{\partial v}{\partial x}\right)^2 \right.$$
$$+ D\left[\left(\frac{\partial^2 w}{\partial x^2}\right)^2 + \left(\frac{\partial^2 w}{\partial y^2} + \frac{w}{R^2}\right)^2 + 2\frac{\partial^2 w}{\partial x^2}\left(\nu\frac{\partial^2 w}{\partial y^2} - \frac{1}{R}\frac{\partial u}{\partial x} - \frac{\nu}{R}\frac{\partial v}{\partial y}\right)\right]$$
$$\left. + \frac{1-\nu}{2}D\left[\left(\frac{\partial^2 w}{\partial x\partial y} + \frac{1}{R}\frac{\partial u}{\partial y}\right)^2 + 3\left(\frac{\partial^2 w}{\partial x\partial y} - \frac{1}{R}\frac{\partial v}{\partial x}\right)^2\right]\right\}, \quad (1)$$

where $C = Eh/(1-\nu^2)$, $D = Ch^2/12$, E is the Young modulus, and ν is the Poisson ratio. The present theory is based on the continuum theory and is applicable to vibrations of wavelength much larger than atomic scale. Although there is anisotropy for materials such as semiconductors, here we treat our structure as being made of an isotropic elastic material for simplicity. The vibrational properties are well described by a model of an isotropic single material even for semiconductor MEMS and NEMS containing multiple layers. (See for example the reports by Yamaguchi *et al.*[25,35]) The strain energy of Eq. (1) is known as Flügge strain energy. For the infinitely small curvature case ($1/R \to 0$), Eq. (1) gives the strain energy for a flat plate. The first line of Eq. (1) shows the extended terms for the in-plane strain energy, and the second and third lines show the extended terms for the out-of-plane strain energy. Eliminating the underlined terms in Eq. (1) gives the strain energy for the shallow shell (or Donnell's) approximation. A typical rolled-up structure of the pseudomorphically strained semiconductor is relaxed by self-rolling, and its equilibrium structure is a cylinder.[36] That is, the total initial stress has already been relaxed and the strain energy for small displacements is written with the second order of expansion of the displacements from the static position, as shown in Eq. (1).[37] The kinetic energy is given by

$$T = \frac{1}{2}\int dx \int d\theta \int_{-h/2}^{h/2} (R+z) dz \rho (\dot{u}^2 + \dot{v}^2 + \dot{w}^2)$$
$$= \frac{1}{2}\int dx dy \rho h (\dot{u}^2 + \dot{v}^2 + \dot{w}^2), \tag{2}$$

where ρ is the mass density. Both U and T are expressed with the displacements on the middle surface. That is, the problem is reduced to a two-dimensional problem on a curved surface of xy coordinates.

By using Hamilton's principle, i.e., minimizing action $\delta \int dt (T-U) = 0$ for a given geometrical configuration, one gets the equation of motion and the boundary conditions for (u,v,w). The equation of motion is written as

$$\rho \frac{\partial^2}{\partial t^2} \boldsymbol{u}(\boldsymbol{r},t) = -\frac{E}{1-\nu^2}(\hat{L}_0 + \hat{L}')\boldsymbol{u}(\boldsymbol{r},t), \tag{3}$$

where $\boldsymbol{u} = (u,v,w)^T$, and

$$\hat{L}_0 = \begin{pmatrix} -\frac{\partial^2}{\partial x^2} - \frac{1-\nu}{2}\frac{\partial^2}{\partial y^2} & -\frac{1+\nu}{2}\frac{\partial^2}{\partial x \partial y} & 0 \\ -\frac{1+\nu}{2}\frac{\partial^2}{\partial x \partial y} & -\frac{1-\nu}{2}\frac{\partial^2}{\partial x^2} - \frac{\partial^2}{\partial y^2} & 0 \\ 0 & 0 & \frac{h^2}{12}\left(\frac{\partial^4}{\partial x^4} + 2\frac{\partial^4}{\partial x^2 \partial y^2} + \frac{\partial^4}{\partial y^4}\right) \end{pmatrix}, \tag{4}$$

$$\hat{L}' = \hat{L}_{\mathrm{D}} + \hat{L}_{\mathrm{F}}, \tag{5}$$

$$\hat{L}_{\mathrm{D}} = \frac{1}{R}\begin{pmatrix} 0 & 0 & -\nu\frac{\partial}{\partial x} \\ 0 & 0 & -\frac{\partial}{\partial y} \\ \nu\frac{\partial}{\partial x} & \frac{\partial}{\partial y} & \frac{1}{R} \end{pmatrix}, \tag{6}$$

$$\hat{L}_{\mathrm{F}} = -\frac{h^2}{12R^2}\begin{pmatrix} \frac{1-\nu}{2}\frac{\partial^2}{\partial y^2} & 0 & -R\frac{\partial^3}{\partial x^3} + \frac{1-\nu}{2}R\frac{\partial^3}{\partial x \partial y^2} \\ 0 & 3\frac{1-\nu}{2}\frac{\partial^2}{\partial x^2} & -\frac{3-\nu}{2}R\frac{\partial^3}{\partial x^2 \partial y} \\ R\frac{\partial^3}{\partial x^3} - \frac{1-\nu}{2}R\frac{\partial^3}{\partial x \partial y^2} & \frac{3-\nu}{2}R\frac{\partial^3}{\partial x^2 \partial y} & -\left(2\frac{\partial^2}{\partial y^2} + \frac{1}{R^2}\right) \end{pmatrix}. \tag{7}$$

As shown in Eqs. (5)–(7), $\hat{L}'$ is the curvature-induced term. Eliminating $\hat{L}_{\mathrm{F}}$ in $\hat{L}'$ gives the equation for the shallow shell approximation. The boundary conditions for our system are summarized in Appendix B.

For the oscillating solution, $\boldsymbol{u}(\boldsymbol{r},t) = \boldsymbol{u}(\boldsymbol{r})e^{i\omega t}$, the equation of motion, Eq. (3), is written as an eigenvalue equation:

$$(\hat{L}_0 + \hat{L}')\boldsymbol{u}(\boldsymbol{r}) = \Lambda \boldsymbol{u}(\boldsymbol{r}), \tag{8}$$

where

$$\Lambda = \frac{\rho}{E/(1-\nu^2)}\omega^2. \tag{9}$$

Instead of solving Eq. (8) with the boundary conditions, the Rayleigh-Ritz method, a variational method to minimize the action with a finite number of bases, has often been used for complicated models. In this paper, we use the Rayleigh-Ritz method to calculate the eigenfunctions and eigenfrequencies numerically. As complementary methods, we also analytically calculate the eigenfunctions and eigenfrequencies with a perturbation method and effective one-dimensional equations of motion.

III. EFFECTS OF CURVATURE ON EIGENFREQUENCY

A. Numerical analysis

The eigenfrequencies are calculated numerically by using the Rayleigh-Ritz method. Polynomial functions are chosen as the base functions. They satisfy a fixed boundary condition along the $y = 0$ edge:

$$u(x,0) = v(x,0) = w(x,0) = \partial_y w(x,0) = 0. \tag{10}$$

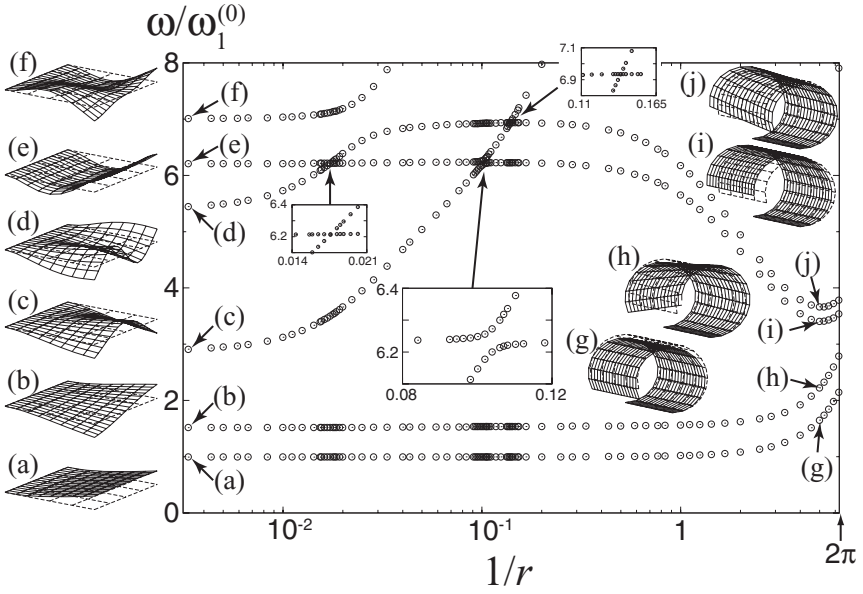

FIG. 2. Eigenfrequencies as a function of curvature. Eigenfrequencies are normalized by fundamental eigenfrequency for wide flat cantilever plate, $\omega_1^{(0)}$. Horizontal axis, $1/r$, is curvature normalized by $1/\ell_y$. Aspect ratios for parameters are $\xi = \ell_x/\ell_y = 2$ and $\eta = h/\ell_y = 2 \times 10^{-3}$, and Poisson ratio $\nu = 0.31$. Insets show larger scale near the arrows. Mode shapes for $1/r = 1/300$ [(a)–(f)] and $1/r = 5$ [(g)–(j)] are shown beside corresponding frequencies. Two straight edges geometrically coincide at $1/r = 2\pi$.

Before discussing the numerical results, we should point out that a scaling law holds for the frequency; i.e., the frequency for each mode is inversely proportional to the system size for the same aspect ratio, $\omega \propto [L^{-1}]$. Hereafter, the unit of length is chosen to be ℓ_y. We use $\xi = \ell_x/\ell_y$, $\eta = h/\ell_y$, and $r = R/\ell_y$ for the normalized lengths.

The calculated eigenfrequencies as a function of curvature are shown in Fig. 2. The frequencies are normalized by the fundamental eigenfrequency of the bending mode for a wide flat cantilever plate:

$$\omega_1^{(0)} = h\left(\frac{\lambda_1^{(0)}}{\ell_y}\right)^2 \sqrt{\frac{E}{12(1-\nu^2)\rho}}, \tag{11}$$

where $\lambda_1^{(0)} = 1.875$. The curvature dependence is shown up to $1/r = 2\pi$, at which point the two straight edges at $\theta = 0$ and ℓ_y/R geometrically coincide. The aspect ratios are $\xi = 2$ and $\eta = 2 \times 10^{-3}$, and the Poisson ratio is 0.31. The mode shapes for small ($1/r = 1/300$) and large ($1/r = 5$) curvature cases are also shown. Note that the normalized frequencies do not depend on the Young modulus or the mass density, but generally depend on the Poisson ratio as well as the aspect ratios (ξ, η, and r). This means that Λ in Eq. (8) corresponds to the normalized frequency and that Λ is determined independently of E and ρ.

For the flat plane limit of $1/r \to 0$, the bending mode in the y direction and the twisting mode correspond to the fundamental and second modes, respectively. The third and fourth modes are the wave modes in the x axis, so the fifth and sixth modes are the second bending and twisting modes, respectively, for this parameter set.

From Fig. 2, one can clearly see two types of curvature effects. When the curvature increases, the eigenfrequencies for the axial wave modes increase even for a small curvature. In contrast, those for the bending and twisting modes remain almost constant. For the large curvature ($1/r > 1$), the eigenfrequencies for these modes show curvature dependence: Those for the lower modes increase as the curvature increases whereas those for the higher modes decrease. Note that the second twisting mode, labeled (f), shows anticrossing with the axial wave mode labeled (d) around $1/r \sim 2 \times 10^{-2}$ and that the twisting mode connects to the mode labeled (j) when the curvature increases. The anticrossing can also be seen between modes (c) and (e) around $1/r \sim 10^{-1}$ although the splitting is smaller. In both cases, the coupled mode functions have the same symmetry with respect to the x axis [even-even for modes (c) and (e), odd-odd for modes (d) and (f)]. The splitting is larger for the modes with higher oscillation in x axis. In contrast, only crossing occurs between modes (d) and (e) and modes (c) and (f) because of the even-odd characteristic of the function set.

As shown in the previous section, the in-plane and out-of-plane modes are no longer separated at the finite curvature. The numerical results show two types of curvature dependence: (I) having higher frequency for the axial wave modes, (II) remaining almost constant for the bending and twisting modes. These two types of curvature dependence are intuitively understandable, and have been shown in previous publications with limited numerical data.[32,33] In the following subsections, the curvature dependence is discussed in more detail along with a perturbation analysis and effective one-dimensional models. The frequencies as a function of the curvature for the axial wave modes are shown to obey a scaling law different from that for the bending and twisting modes.

B. Perturbation analysis

For further quantitative and physical discussion of the numerical calculation above, we apply perturbation analysis to the equation of motion. The curvature effect is estimated by considering $\hat{L}'$ as the perturbation of $\hat{L}_0$ in Eq. (8). For this analysis, we consider the perturbation for plane wave with wave vector $\boldsymbol{k} = (k_x, k_y)$, which is the eigenfunction in the periodic boundary condition, within the shallow shell approximation for simplicity. The derivation of the results shown in this subsection is given in detail in Appendix C.

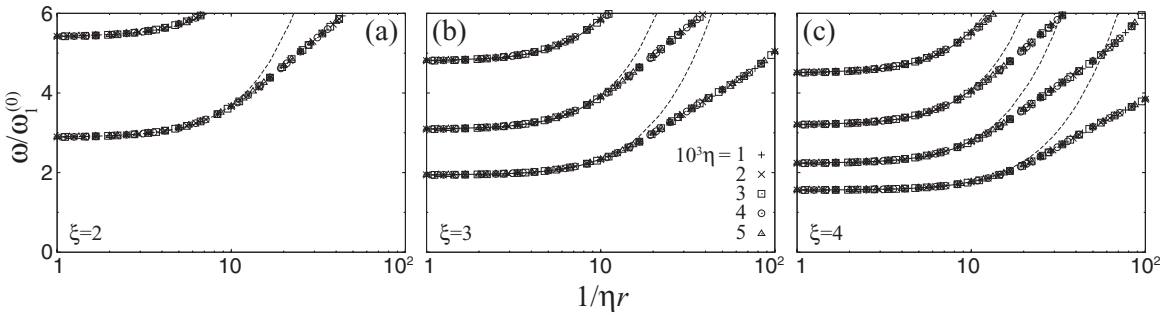

FIG. 3. Normalized frequencies for axial wave modes as function of $1/\eta r$ for three aspect ratios: (a) $\xi = 2$, (b) $\xi = 3$, (c) $\xi = 4$. Results for five thicknesses of η are shown. Poisson ratio $\nu = 0.31$. Dashed lines are curves fitting analytical expression, Eq. (13).

The eigenfrequency of the out-of-plane mode for the plane wave is given by

$$\omega_{\mathrm{OP}}^{(0)} = hk^2\sqrt{\frac{E}{12(1-\nu^2)\rho}}, \tag{12}$$

where $k = \sqrt{k_x^2 + k_y^2}$. At finite curvature, the in-plane and out-of-plane modes are no longer separated. The curvature-induced frequency modification is evaluated within the second-order perturbation of the curvature as

$$\omega_{\mathrm{OP}} = \omega_{\mathrm{OP}}^{(0)}\sqrt{1 + 12(1-\nu^2)\frac{k_x^4}{k^8 h^2 R^2}}. \tag{13}$$

See Appendix C for the derivation. A corresponding expression is obtained by neglecting the tangential inertia terms in the shallow shell approximation for the all-edges-simply-supported boundary condition[38] or for the closed cylindrical shell with the both-ends-simply-supported condition.[26] As shown in Eq. (13), the curvature modification appears as $1/R^2$, and the effect is larger for a larger k_x. Note that the curvature effect does not appear for the $k_x = 0$ modes, only for the axial wave modes. Also note that the $k_x = 0$ modes correspond to the bending modes. These behaviors agree with the numerical calculation results shown in Fig. 2.

Let us consider the curvature dependence of the frequencies for the axial wave modes from Eq. (13). Although Eq. (13) is the expression for the plane wave, we could expect that (i) the normalized frequency is a function of hR and (ii) the vector set of $\boldsymbol{k}$ is given for each mode as an "effective" wave vector for the rolled-up cantilever shell. We confirm these nontrivial hypotheses by plotting the numerically calculated frequencies for the axial wave modes as a function of $1/\eta r$ for various aspect ratios of η and ξ with $\nu = 0.31$ in Fig. 3. The dashed lines show the fitting to Eq. (13) using $\boldsymbol{k} = (k_x, k_y)$ as the fitting parameters. We strongly emphasize that the frequency as a function of the curvature for each mode is scaled by a single function of $1/\eta r$ for given ξ, even for the larger curvature in which the expression of Eq. (13) deviates from the numerical calculation.

There is also a correction for the $k_x = 0$ mode function. The corrections for the frequency cancel each other for the $k_x = 0$ mode in this approximation. However, the $k_x = 0$ out-of-plane mode function is modified, and the following inextensionality relation is satisfied (see Appendix C for details):

$$\frac{\partial v}{\partial y} + \frac{w}{R} = 0. \tag{14}$$

Note that the normal strain in the curved y direction is written as $\varepsilon_y = \partial_y v + w/R$. For the $k_x \neq 0$ modes, in-plane extension is induced by the curvature, so the frequency is significantly enhanced. Note that the twisting modes can be classified neither as $k_x = 0$ nor $k_x \neq 0$ in the plane wave picture. The inextensionality relation is also applicable to twisting modes, as shown in the next subsection.

C. One-dimensional vibration in circumference direction

Here we focus on the bending and twisting modes. As shown in the numerical calculation, these modes show curvature dependence for larger curvatures; lower modes increase whereas higher modes decrease when the curvature increases. Here we show that effective one-dimensional models reproduce the numerical calculation quite well. A scaling law for these modes is also discussed.

For the bending modes, we make several assumptions: Inextensionality relations $\partial_x u = 0$, $\partial_y u + \partial_x v = 0$, $\partial_y v + w/R = 0$, and x dependence is neglected ($\partial_x \boldsymbol{u} = 0$). By applying these assumptions to the strain energy of Eq. (1) and using Hamilton's principle, we get a one-dimensional equation of motion:

$$v^{(6)} + \frac{2v^{(4)}}{r^2} + \frac{v^{(2)}}{r^4} = \lambda^4\left(v^{(2)} - \frac{v}{r^2}\right), \tag{15}$$

with boundary conditions

$$v = v' = v^{(2)} = 0, \quad (\psi = 0), \tag{16}$$

$$\begin{aligned} v^{(3)} + \frac{v'}{r^2} &= v^{(4)} + \frac{v^{(2)}}{r^2} \\ &= v^{(5)} + \frac{2v^{(3)}}{r^2} + \left(\frac{1}{r^4} - \lambda^4\right)v' = 0, \quad (\psi = 1), \end{aligned} \tag{17}$$

where the dimensionless coordinate $\psi = y/\ell_y$ is introduced, the derivative is for ψ, and

$$\lambda^4 = \frac{12(1-\nu^2)\rho}{E}\frac{\ell_y^4}{h^2}\omega^2. \tag{18}$$

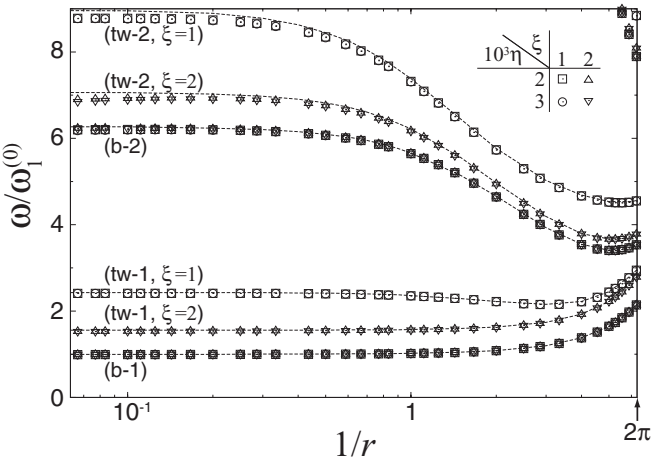

FIG. 4. Normalized frequencies of lowest and first excited bending modes (b-1) and (b-2) and lowest and first excited twisting modes (tw-1) and (tw-2) for numerical calculation (plot points) as function of $1/r$ for various values of ξ and η. Poisson ratio $\nu = 0.31$. Frequencies for bending and twisting modes calculated using effective one-dimensional models are shown by dashed lines.

Note that the equation of motion of Eq. (15) has the same form as a curved beam (see for example the review article by Chidamparam and Leissa[39]). A general solution of Eq. (15) has the form

$$v(\psi) = \sum_{j=1}^{N} (A_j \cos k_j \psi + B_j \sin k_j \psi), \tag{19}$$

where $N = 3$ and k_j's are the roots of the equation

$$k^6 - \frac{2}{r^2}k^4 + \left(\frac{1}{r^4} - \lambda^4\right)k^2 - \frac{\lambda^4}{r^2} = 0, \tag{20}$$

which is given by substituting Eq. (19) into Eq. (15). Similar to the straight cantilever problem, the eigenfrequencies are calculated by using the boundary conditions and then evaluating the roots of the determinant of the matrix for vector $(A_1, \ldots, B_3)$.

The frequencies calculated using Eqs. (15)–(17) are plotted in Fig. 4. The numerical calculation of the bending modes is well reproduced by the one-dimensional equation of motion. The normalized frequencies for the numerical calculation perfectly follow function of $1/r$ independently of the values of η and ξ. This scaling law is derived that Eqs. (15)–(17) depend only on r. Note that the normalized frequency in the analytical expression is written as $\omega/\omega_1^{(0)} = (\lambda/\lambda_1^{(0)})^2$.

For the twisting modes, we make similar assumptions about the bending modes, i.e., the inextensionality relation and the antisymmetric mode shape of $v(x,y) \propto x v(y)$. We get a quasi-one-dimensional equation of motion:

$$u^{(8)} + 2\left(\frac{1}{r^2} - \alpha\right)u^{(6)} + \left(\frac{1}{r^4} - \frac{4\alpha}{r^2}\right)u^{(4)} - \frac{2\alpha u^{(2)}}{r^4} = \lambda^4\left(u^{(4)} - \frac{u^{(2)}}{r^2} + \frac{\beta u}{r^2}\right), \tag{21}$$

where $\alpha = 12(1-\nu)/\xi^2$, $\beta = 12/\xi^2$, and the boundary conditions are

$$u = u' = u^{(2)} = u^{(3)} = 0 \tag{22}$$

for $\psi = 0$, and

$$\begin{aligned} u^{(4)} + \frac{u^{(2)}}{r^2} &= u^{(5)} + \left(\frac{1}{r^2} - 2\alpha\right)u^{(3)} - \frac{2\alpha u'}{r^2} \\ &= u^{(6)} + 2\left(\frac{1}{r^2} - \alpha\right)u^{(4)} + \left(\frac{1}{r^4} - \frac{2\alpha}{r^2} - \lambda^4\right)u^{(2)} \\ &= u^{(7)} + 2\left(\frac{1}{r^2} - \alpha\right)u^{(5)} + \left(\frac{1}{r^4} - \frac{4\alpha}{r^2} - \lambda^4\right)u^{(3)} \\ &\quad - \frac{1}{r^2}\left(\frac{2\alpha}{r^2} - \lambda^4\right)u' = 0 \end{aligned} \tag{23}$$

for $\psi = 1$. A general solution of Eq. (21) has the same form as Eq. (19) with $N = 4$.

In a similar way as for the bending modes, the frequencies of the twisting modes are calculated from Eqs. (21)–(23). They are also shown in Fig. 4. The numerical calculation of the twisting modes is well reproduced by the quasi-one-dimensional equation of motion, and the normalized frequencies are fitted by the function of $1/r$ for the given ξ, independently of η.

We would like to emphasize that the scaling law of the functions of $1/r$ for the bending and twisting modes are in contrast to the scaling law of the functions of $1/\eta r$ for the axial wave modes. More precisely, the curvature dependence of the normalized frequency $\omega_j/\omega_1^{(0)}$ for each mode labeled j is written as $\omega_{j_b}/\omega_1^{(0)} = f_{b,j_b}(1/r)$ for bending mode j_b, $\omega_{j_t}/\omega_1^{(0)} = f_{t,j_t}(1/r;\xi)$ for twisting mode j_t, and $\omega_{j_a}/\omega_1^{(0)} = f_{a,j_a}(1/\eta r;\xi)$ for axial wave mode j_a.

IV. ELECTROMECHANICAL COUPLING

For microfabricated freestanding semiconductor structures used as micro- and nano-electromechanical systems, the coupling between the mechanical vibration and the 2DEG would affect both the vibrational and electrical properties. Here we briefly discuss several possible mechanisms of electromechanical coupling.

We first discuss a capacitive coupling mechanism. We consider a doping layer with a positive charge at $z = d/2$ and a negatively charged 2DEG layer of the same absolute charge density with the doping layer at $z = -d/2$. We first consider a flat plate. A displacement causes a finite curvature of $1/\delta r$ in a local area, and this modifies the local capacitance per unit area:

$$c = \frac{\varepsilon}{\delta r}\frac{1}{\ln\frac{1+d/2\delta r}{1-d/2\delta r}} \simeq \frac{\varepsilon}{d}\frac{1}{1+\frac{d^2}{12\delta r^2}}, \tag{24}$$

where ε is the dielectric constant. The finite curvature at a position is written with displacement represented as $\delta r^{-1} \simeq (d^2w/dy^2)$. Therefore, the capacitive coupling energy density induced by the displacement can be expressed as

$$\epsilon_c = \frac{(ne)^2}{2c} - \frac{(ne)^2}{2c_{\delta r=\infty}} = \frac{n^2e^2d^3}{24\varepsilon}\left(\frac{d^2w}{dy^2}\right)^2, \tag{25}$$

where n is the charge density and $-e$ is the electron charge. This expression can be directly compared with the strain energy density,

$$\epsilon_s = \frac{Eh^3}{24(1-\nu^2)}\left(\frac{d^2w}{dy^2}\right)^2. \tag{26}$$

From Eqs. (25) and (26), we can see that the capacitive coupling effect is larger for thinner plate, $h \sim d$. However, for typical systems with parameters $n \sim 7 \times 10^{15}$ m^{-2}, $\varepsilon \sim 9 \times 10^{-11}$ N/V^2, $E \sim 9 \times 10^{10}$ N/m^2, and $\nu = 0.3$, we can estimate the ratio as $\epsilon_c/\epsilon_s \sim 10^{-7}$ for $h \sim d$.

For the rolled-up systems, the energy density is expressed in a manner similar to that for a flat plate: The corresponding expression is obtained by changing (d^2w/dy^2) in Eq. (25) to $(d^2w/dy^2 + w/R^2)$. The strain energy density is expressed in the same manner. Therefore, we come to the same conclusion as for the flat plate. That is, the capacitive coupling has a negligible effect on the vibration frequency, even for a thin rolled-up plate. However, the coupling would significantly affect the electron systems. The prefactor in Eq. (25) is the order of eV for the parameters used above. A mechanical vibration with an amplitude of nm order and a wavelength of μm order in a 10×10 μm area would induce a capacitive coupling energy of the order of sub-millielectron volt. This is the same order as that of typical single-particle energy separation and Coulomb interaction for mesoscopic electron systems. Therefore, the capacitive coupling could affect 2DEG systems, even for a flat plate.

Microscopic electron-vibration (i.e., phonon) interaction could show a mode dependence for the interaction effect. The interaction via the deformation potential is written as

$$V = g \int \rho_e(\boldsymbol{r}) \Delta(\boldsymbol{r}) d\boldsymbol{r}, \tag{27}$$

where $\rho_e(\boldsymbol{r})$ is the density of electrons, $\Delta(\boldsymbol{r})$ is the local compression or extension, and g is the coupling constant. For the 2DEG layer at the z surface,

$$\Delta(\boldsymbol{r}) \simeq \frac{\partial u}{\partial x} + \frac{\partial v}{\partial y} + \frac{w}{R} - z\left(\frac{\partial^2 w}{\partial x^2} + \frac{\partial^2 w}{\partial y^2}\right). \tag{28}$$

Let us consider the 2DEG layer near the middle surface at $z = 0$. For the bending and twisting modes, the potential would be negligible because of the inextensionality; i.e., $\Delta \simeq 0$. In contrast, the axial wave modes would induce the in-plane extension, as discussed in Sec. III, resulting in strong interaction between electrons. The interaction would appear as several effects: The long-range potential created by the vibrational modes would modify the local electron density, and the lowest order of the interaction would dampen the vibration.[25] Therefore, the quality factor for each resonant frequency would reflect the mode shape.

In the above discussion, we neglected the piezoelectric effect. A rolled-up semiconductor still has local strain in a static situation.[40] Depending on the rolling direction, e.g., [110] for zinc-blende materials, a strain-induced polarization charge would appear via the piezoelectric effect. A total strain energy calculation shows that [100] is the preferred rolling direction for such materials;[36] therefore, this effect seems to be ignored. However, superlattices[41] and rolled-up semiconductors have less geometrical symmetry than bulk crystal. This might induce a finite piezoelectric field in the direction in which the piezoelectric effect does not normally occur for bulk materials. A careful microscopic study is needed to clarify the piezoelectric effect.

In the presence of a magnetic field, one would also expect an electromechanical coupling via the magnetic field. For instance, out-of-plane vibration changes the perpendicular magnetic field on the surface coordinate system, resulting in an eddy current due to electromagnetic induction. This eddy current can be used as a signal for vibration detection.[42] This eddy current would interact with the magnetic field and would serve as a damping effect.[43]

This damping mechanism can be captured with a simplified model. Consider a rectangular wire pendulum with deflection angle φ. The equation of motion of the pendulum is

$$I\frac{d^2\varphi}{dt^2} = -I\omega_0^2\varphi, \tag{29}$$

where I is the inertia moment of the pendulum with respect to the fixed edge and ω_0 is the frequency of the pendulum. An external magnetic field is applied with angle θ_B to the equilibrium position of the pendulum plane. The oscillation changes the magnetic flux penetrating the wire, which induces electromotive force and results in a current flow in the wire: $J = (SB/R)\cos(\theta_B - \varphi)\dot{\varphi}$, where S is the area of the wire and R is its electrical resistance. The current interacts with the magnetic field via the Ampere force, creating torque on the pendulum. For a small oscillation amplitude ($\varphi \ll \theta_B$), the equation of motion is

$$\frac{d^2\varphi}{dt^2} = -\omega_0^2\varphi - \frac{S^2B^2}{IR}\cos^2\theta_B\frac{d\varphi}{dt}. \tag{30}$$

The second term on the right is the damping term. For a flat cantilever plate, the electromagnetic coupling can be changed by changing the direction of the magnetic field. It is small when the magnetic field is perpendicular to the plate ($\theta_B = \pi/2$). For a rolled-up system, the electromagnetic coupling should contribute for any direction of the magnetic field. This can be expressed by simply integrating the θ_B dependence for the sample as represented in Eq. (30). Doing this, we get the phenomenological expression for the rolled-up system:

$$\frac{d^2\varphi}{dt^2} = -\omega_0^2\varphi - cB^2\frac{d\varphi}{dt}. \tag{31}$$

The constant c would depend not only on the geometry of the system but also on the modes. For a strong magnetic field, the additional contribution from the quantum Hall effect should also be considered.[25]

V. DISCUSSION AND SUMMARY

The mechanical vibrations in flat semiconductor layers have been observed using electrical transport measurement[2] and laser interferometer measurement.[10] Rolled-up semiconductor layers have been fabricated, and their electronic properties have been investigated.[16,18] It would be useful to show the frequencies around the fundamental frequency for the corresponding structure. For $\ell_x = 1000$ μm, $\ell_y = 100$ μm, $R = 20$ μm, and $h = 0.2$ μm, similar to the parameter settings in previous work,[16,18] and using the GaAs material constants $E = 8.59 \times 10^{10}$ N/m^2, $\nu = 0.31$, and $\rho = 5.32 \times 10^3$ kg/m^3, we calculated the fundamental eigenfrequency as $f = \omega/2\pi = 22.53$ kHz and calculated 23.09, 46.55, and 46.65 kHz for the excited modes, respectively the lowest bending, lowest twisting, first excited bending, and first excited twisting modes. Because the rolled-up structure had a long axis, $\xi = \ell_x/\ell_y =$

10, the bending mode and corresponding twisting mode had closer frequencies. These resonant frequencies would be expected in future experiments.

In this paper we restricted ourselves to classical physics; however, an important issue related to NEMS is the quantum effect.[8] The results presented here can be used to estimate the condition for observing a quantum effect on the fundamental frequency of rolled-up semiconductor layers. The energy quantum of the fundamental frequency should be larger than the thermal excitation. As shown in Fig. 2, the fundamental frequency is increased by the curvature, and the frequency is approximately twice that of the cantilever plate $\omega_1/\omega_1^{(0)} \simeq 2$, near the ring shape $R \simeq \ell_y/2\pi$. For example, for GaAs layer thickness $h = 50$ nm and circumference length $\ell_y = 10h = 500$ nm, the fundamental eigenfrequency for the layer rolled-up in a ring shape is $f_1 = \omega_1/2\pi \simeq 270$ MHz. The corresponding temperature is about 10 mK, which could be achieved with a dilution refrigerator.

In summary, we have studied the mechanical vibration of a cylindrically rolled-up cantilever shell. We have shown that the axial wave modes have higher frequencies when curvature is induced while the bending and twisting modes have weaker curvature dependence. The axial wave modes obey a scaling law different from that for the bending and twisting modes. Several possible electromechanical coupling mechanisms were considered.

ACKNOWLEDGMENTS

The authors would like to thank F. Grosse, M. Hanke, P. V. Santos, and R. Hey for their useful discussions with us about mechanical vibration. This work was supported by the DFG-JST Strategic Japanese-German Cooperative Program on "Nanoelectronics" (No. FR 930/16-1 and No. AOBJ 548229) and partly supported by Grants-in-Aid (No. 22740191 and No. 23241046) from the Ministry of Education, Culture, Sports, Science, and Technology, Japan.

APPENDIX A: STRAIN ENERGY IN FLÜGGE SHELL THEORY

In this Appendix, we explain the derivation of the strain energy in Flügge shell theory.

Under the Kirchhoff-Love approximation ("normals to the undeformed middle surface remain straight and normal to the deformed middle surface and suffer no extension"), each component of the displacement at any point in the thickness of the shell can be expressed using the displacements at the middle surface:

$$u(z) = u - z\frac{\partial w}{\partial x}, \tag{A1}$$

$$v(z) = v\left(1 + \frac{z}{R}\right) - \frac{z}{R}\frac{\partial w}{\partial \theta}, \tag{A2}$$

$$w(z) = w, \tag{A3}$$

where u, v, and w are the displacement components in the x, θ, and z directions at the middle surface, respectively, and $u(z)$, $v(z)$, and $w(z)$ represent the corresponding displacements at the z surface. The strain tensors at a point within the thickness are given by

$$\varepsilon_x = \frac{\partial u(z)}{\partial x}, \tag{A4}$$

$$\varepsilon_\theta = \frac{\partial v(z)}{(R+z)\partial\theta} + \frac{w(z)}{R+z}, \tag{A5}$$

$$\gamma_{x\theta} = \frac{\partial v(z)}{\partial x} + \frac{\partial u(z)}{(R+z)\partial\theta}. \tag{A6}$$

The second term in Eq. (A2) and the second term in Eq. (A5) appear because the coordinates sit on a curved surface. The transverse shear strains, γ_{xz} and $\gamma_{\theta z}$, and the transverse normal strain, ε_z, are assumed to be zero in the Kirchhoff-Love approximation. The strain energy is given by

$$U = \frac{1}{2}\int dx \int d\theta \int_{-h/2}^{h/2} (R+z)dz \times \left[\frac{E}{1-\nu^2}\left(\varepsilon_x^2 + \varepsilon_\theta^2 + 2\nu\varepsilon_x\varepsilon_\theta\right) + \frac{E}{2(1+\nu)}\gamma_{x\theta}^2\right], \tag{A7}$$

where E is the Young modulus and ν is the Poisson ratio. Substituting Eqs. (A4)–(A6) with the relations (A1)–(A3) into Eq. (A7) and integrating out the z component gives the strain energy with the displacements at the middle surface [Eq. (1)]. To perform the z component integration, the z/R terms in the denominator of Eqs. (A5) and (A6) were expanded up to the second order, and the terms up to third order of h were remained in the strain energy.

APPENDIX B: BOUNDARY CONDITIONS

Here we summarize the boundary conditions for the presented system. The system has free boundaries at the $x = \pm\ell_x/2$ and $y = \ell_y$ edges and a fixed boundary at the $y = 0$ edge. The boundary conditions at each edge can be determined using Hamilton's principle as the same framework for deriving the equation of motion. For the fixed boundary edge at $y = 0$, we have $u = v = w = \partial w/\partial y = 0$ as the boundary conditions. For the free boundaries at $x = \pm\ell_x/2$, the boundary conditions are

$$\frac{\partial u}{\partial x} + \nu\left(\frac{\partial v}{\partial y} + \frac{w}{R}\right) - \frac{h^2}{12R^2}R\frac{\partial^2 w}{\partial x^2} = 0, \tag{B1}$$

$$\frac{\partial u}{\partial y} + \left(1 + 3\frac{h^2}{12R^2}\right)\frac{\partial v}{\partial x} - 3\frac{h^2}{12R^2}R\frac{\partial^2 w}{\partial x\partial y} = 0, \tag{B2}$$

$$\frac{1}{R}\left(-\frac{\partial^2 u}{\partial x^2} + \frac{1-\nu}{2}\frac{\partial^2 u}{\partial y^2} - \frac{3-\nu}{2}\frac{\partial^2 v}{\partial x\partial y}\right) + \frac{\partial^3 w}{\partial x^3} + (2-\nu)\frac{\partial^3 w}{\partial x\partial y^2} = 0, \tag{B3}$$

$$\frac{1}{R}\left(\frac{\partial u}{\partial x} + \nu\frac{\partial v}{\partial y}\right) - \frac{\partial^2 w}{\partial x^2} - \nu\frac{\partial^2 w}{\partial y^2} = 0. \tag{B4}$$

At $y = \ell_y$, the boundary conditions are

$$\left(1 + \frac{h^2}{12R^2}\right)\frac{\partial u}{\partial y} + \frac{\partial v}{\partial x} + \frac{h^2}{12R^2}R\frac{\partial^2 w}{\partial x\partial y} = 0, \tag{B5}$$

$$\nu\frac{\partial u}{\partial x}+\frac{\partial v}{\partial y}+\left(1+\frac{h^2}{12R^2}\right)\frac{w}{R}+\frac{h^2}{12R^2}R\frac{\partial^2 w}{\partial y^2}=0, \quad \text{(B6)}$$

$$\frac{1}{R}\frac{1-\nu}{2}\left(\frac{\partial^2 u}{\partial x\partial y}-3\frac{\partial^2 v}{\partial x^2}\right)+\frac{\partial^3 w}{\partial y^3}+(2-\nu)\frac{\partial^3 w}{\partial x^2\partial y}+\frac{1}{R^2}\frac{\partial w}{\partial y}=0, \quad \text{(B7)}$$

$$\nu\frac{\partial^2 w}{\partial x^2}+\frac{\partial^2 w}{\partial y^2}+\frac{w}{R^2}=0. \quad \text{(B8)}$$

APPENDIX C: PERTURBATION ANALYSIS

Here we use perturbation theory to evaluate the analytical expression for the curvature-induced frequency. To keep the analysis simple, we consider the plane wave specified by $\boldsymbol{k}=(k_x,k_y)$ for the mode and consider the curvature-induced term only within the shallow shell approximation; i.e., the $\hat{L}_{\rm F}$ term is neglected in the $\hat{L}'$ term in Eq. (5). The unperturbed eigenfrequencies and eigenfunctions are

$$\omega^{(0)}_{\rm LA}=\sqrt{\frac{E}{(1-\nu^2)\rho}}k,$$
$$\boldsymbol{u}^{(0)}_{\rm LA}=\frac{1}{\sqrt{l_x l_y}}(\cos\theta_{\boldsymbol{k}}\boldsymbol{e}_x+\sin\theta_{\boldsymbol{k}}\boldsymbol{e}_y)\exp(i\boldsymbol{k}\cdot\boldsymbol{r}), \quad \text{(C1)}$$

$$\omega^{(0)}_{\rm TA}=\sqrt{\frac{E}{2(1+\nu)\rho}}k,$$
$$\boldsymbol{u}^{(0)}_{\rm TA}=\frac{1}{\sqrt{l_x l_y}}(-\sin\theta_{\boldsymbol{k}}\boldsymbol{e}_x+\cos\theta_{\boldsymbol{k}}\boldsymbol{e}_y)\exp(i\boldsymbol{k}\cdot\boldsymbol{r}), \quad \text{(C2)}$$

$$\omega^{(0)}_{\rm OP}=h\sqrt{\frac{E}{12(1-\nu^2)\rho}}k^2, \quad \boldsymbol{u}^{(0)}_{\rm OP}=\frac{1}{\sqrt{l_x l_y}}\boldsymbol{e}_z\exp(i\boldsymbol{k}\cdot\boldsymbol{r}), \quad \text{(C3)}$$

where $k=\sqrt{k_x^2+k_y^2}$, $\boldsymbol{e}_x$ ($\boldsymbol{e}_y$, $\boldsymbol{e}_z$) is the unit vector in the x (y, z) direction, and $\theta_{\boldsymbol{k}}=\arctan(k_y/k_x)$. Equations (C1)–(C3) respectively represent the in-plane longitudinal, in-plane transverse, and out-of-plane modes. Each eigenfunction is normalized in the $\ell_x\times\ell_y$ square. The calculated first- and second-order perturbation corrections for the out-of-plane mode are

$$\Lambda^{(1)}_{\rm OP}=\int d\boldsymbol{r}\boldsymbol{u}^{(0)*}_{\rm OP}\hat{L}'\boldsymbol{u}^{(0)}_{\rm OP}=\frac{1}{R^2}, \quad \text{(C4)}$$

$$\Lambda^{(2)}_{\rm OP}=-\sum_j\frac{\left|\int d\boldsymbol{r}\boldsymbol{u}^{(0)*}_j\hat{L}'\boldsymbol{u}^{(0)}_{\rm OP}\right|^2}{\Lambda^{(0)}_j-\Lambda^{(0)}_{\rm OP}}=-\frac{1}{R^2}\left\{1-(1-\nu^2)\left(\frac{k_x}{k}\right)^4\right\}, \quad \text{(C5)}$$

where summation j in Eq. (C5) is taken for $j=$ LA,TA, and relation $\Lambda^{(0)}_j-\Lambda^{(0)}_{\rm OP}\simeq\Lambda^{(0)}_j$ is used to obtain the final expression of Eq. (C5). Using Eqs. (C4) and (C5), we calculate the effect of the curvature on the frequency:

$$\omega_{\rm OP}=\omega^{(0)}_{\rm OP}\sqrt{1+12(1-\nu^2)\frac{k_x^4}{k^8h^2R^2}}. \quad \text{(C6)}$$

In this equation, the curvature modification appear as $1/R^2$, and the effect is larger for a larger k_x.

There is also a correction for the $k_x=0$ modes. As can be seen from Eqs. (C4) and (C5), the first- and second-order perturbations for the frequency completely cancel each other for the $k_x=0$ modes. The $k_x=0$ out-of-plane mode function is modified within the first order of $\hat{L}'$ as

$$\boldsymbol{u}_{\rm OP}=\boldsymbol{u}^{(0)}_{\rm OP}-\sum_j\frac{\int d\boldsymbol{r}\boldsymbol{u}^{(0)*}_j\hat{L}'\boldsymbol{u}^{(0)}_{\rm OP}}{\Lambda^{(0)}_j-\Lambda^{(0)}_{\rm OP}}\boldsymbol{u}^{(0)}_j=\frac{1}{\sqrt{l_x l_y}}\left(\boldsymbol{e}_z-\frac{1}{ik_yR}\boldsymbol{e}_y\right)\exp(ik_y y). \quad \text{(C7)}$$

Therefore, the inextensionality relation, Eq. (14), holds for the $k_x=0$ modes.

*izumida@cmpt.phys.tohoku.ac.jp

[1] A. N. Cleland, *Foundations of Nanomechanics* (Springer, Berlin, 2002).

[2] H. Yamaguchi, Y. Tokura, S. Miyashia, and Y. Hirayama, Phys. Rev. Lett. **93**, 036603 (2004).

[3] N. Lambert, I. Mahboob, M. Pioro-Ladrière, Y. Tokura, S. Tarucha, and H. Yamaguchi, Phys. Rev. Lett. **100**, 136802 (2008).

[4] J. P. Eisenstein, H. L. Stormer, V. Narayanamurti, A. Y. Cho, A. C. Gossard, and C. W. Tu, Phys. Rev. Lett. **55**, 875 (1985).

[5] J. G. E. Harris, R. Knobel, K. D. Maranowski, A. C. Gossard, N. Samarth, and D. D. Awschalom, Phys. Rev. Lett. **86**, 4644 (2001).

[6] N. Ruhe, G. Stracke, C. Heyn, D. Heitmann, H. Hardtdegen, T. Schäpers, B. Rupprecht, M. A. Wilde, and D. Grundler, Phys. Rev. B **80**, 115336 (2009).

[7] A. Naik, O. Buu, M. D. LaHaye, A. D. Armour, A. A. Clerk, M. P. Blencowe, and K. C. Schwab, Nature (London) **443**, 193 (2006).

[8] A. D. O'Connell, M. Hofheinz, M. Ansmann, R. C. Bialczak, M. Lenander, E. Lucero, M. Neeley, D. Sank, H. Wang, M. Weides, J. Wenner, J. M. Martinis, and A. N. Cleland, Nature (London) **464**, 697 (2010).

[9] J. Stettenheim, M. Thalakulam, F. Pan, M. Bal, Z. Ji, W. Xue, L. Pfeiffer, K. W. West, M. P. Blencowe, and A. J. Rimberg, Nature (London) **466**, 86 (2010).

[10] H. Okamoto, D. Ito, K. Onomitsu, H. Sanada, H. Gotoh, T. Sogawa, and H. Yamaguchi, Phys. Rev. Lett. **106**, 036801 (2011).

[11] V. Y. Prinz, V. A. Seleznev, A. K. Gutakovsky, A. V. Chehovskiy, V. V. Preobrazhenskii, M. A. Putyato, and T. A. Gavrilova, Physica E **6**, 828 (2000).

[12] V. Y. Prinz, V. A. Seleznev, A. V. Prinz, and A. V. Kopylov, Sci. Technol. Adv. Mater. **10**, 034502 (2009).

[13]T. Kipp, H. Welsch, C. Strelow, C. Heyn, and D. Heitmann, Phys. Rev. Lett. **96**, 077403 (2006).
[14]S. Mendach, R. Songmuang, S. Kiravittaya, A. Rastelli, M. Benyoucef, and O. G. Schmidt, Appl. Phys. Lett. **88**, 111120 (2006).
[15]N. Shaji, H. Qin, R. H. Blick, L. J. Klein, C. Deneke, and O. G. Schmidt, Appl. Phys. Lett. **90**, 042101 (2007).
[16]K.-J. Friedland, R. Hey, H. Kostial, A. Riedel, and K. H. Ploog, Phys. Rev. B **75**, 045347 (2007).
[17]A. B. Vorob'ev, K.-J. Friedland, H. Kostial, R. Hey, U. Jahn, E. Wiebicke, J. S. Yukecheva, and V. Y. Prinz, Phys. Rev. B **75**, 205309 (2007).
[18]K.-J. Friedland, A. Siddiki, R. Hey, H. Kostial, A. Riedel, and D. K. Maude, Phys. Rev. B **79**, 125320 (2009).
[19]R. Saito, G. Dresselhaus, and M. S. Dresselhaus, *Physical Properties od Carbon Nanotubes* (Imperial College Press, London, 1998).
[20]E. Prada, P. San-Jose, and L. Brey, Phys. Rev. Lett. **105**, 106802 (2010).
[21]D. Rainis, F. Taddei, M. Polini, G. León, F. Guinea, and V. I. Fal'ko, Phys. Rev. B **83**, 165403 (2011).
[22]X. Xie, L. Ju, X. Feng, Y. Sun, R. Zhou, K. Liu, S. Fan, Q. Li, and K. Jiang, Nano Lett. **9**, 2565 (2009).
[23]Y. Gao, X. Chen, H. Xu, Y. Zou, R. Gu, M. Xu, A. K.-Y. Jen, and H. Chen, Carbon **48**, 4475 (2010).
[24]K. Jensen, K. Kim, and A. Zettl, Nature Nanotechnology **3**, 533 (2008).
[25]H. Yamaguchi, H. Okamoto, Y. Maruta, S. Ishihara, S. Miyashita, and Y. Hirayama, Jpn. J. Appl. Phys. **46**, L658 (2007).
[26]A. W. Leissa, *Vibration of Shells*, NASA SP-288 (National Aeronautics and Space Administration, Washington, DC, 1973).
[27]M. Qatu, Shock. Vib. Dig. **24**, 3 (1992).
[28]K. M. Liew, C. W. Lim, and S. Kitipornchai, Appl. Mech. Rev. **50**, 431 (1997).
[29]M. S. Qatu, Appl. Mech. Rev. **55**, 325 (2002).
[30]M. S. Qatu, Appl. Mech. Rev. **55**, 415 (2002).
[31]M. S. Qatu, R. W. Sullivan, and W. Wang, Compos. Struct. **93**, 14 (2010).
[32]A. Leissa, J. Lee, and A. Wang, Int. J. Solids. Struct. **19**, 411 (1983).
[33]K. M. Liew and C. W. Lim, Acta Mech. **114**, 95 (1996).
[34]Y. Narita and P. Robinson, Int. J. Mech. Sci. **48**, 1516 (2006).
[35]H. Yamaguchi, K. Kato, Y. Nakai, K. Onomitsu, S. Warisawa, and S. Ishihara, Appl. Phys. Lett. **92**, 251913 (2008).
[36]M. Grundmann, Appl. Phys. Lett. **83**, 2444 (2003).
[37]In a rolled-up pseudomorphically strained semiconductor, there should still be a microscopic strain in each layer. This local strain would couple to the displacement via anharmonic constants (Refs. 44–46), and the effect would renormalize the elastic constant. The typical local strain in a rolled-up semiconductor structure is 10^{-2}, and the anharmonic contribution to the harmonic constant is estimated to be less than about 10%, which could be negligible in the first approximation.
[38]A. Leissa and A. Kadi, J. Sound. Vib. **16**, 173 (1971).
[39]P. Chidamparam and A. W. Leissa, Appl. Mech. Rev. **46**, 467 (1993).
[40]R. Hey, M. Ramsteiner, P. Santos, and K.-J. Friedland, J. Cryst. Growth **311**, 1680 (2009).
[41]S. Adachi, *GaAs and Related Materials* (World Scientific, Singapore, 1994).
[42]A. N. Cleland and M. L. Roukes, Appl. Phys. Lett. **69**, 2653 (1996).
[43]X. M. H. Huang, X. L. Feng, C. A. Zorman, M. Mehregany, and M. L. Roukes, New J. Phys. **7**, 247 (2005).
[44]J. R. Drabble and A. J. Brammer, Solid State Commun. **4**, 467 (1966).
[45]H. J. McSkimin and P. Andreatch, J. Appl. Phys. **38**, 2610 (1967).
[46]Y. Abe and K. Imai, Jpn. J. Appl. Phys. Suppl. **25**, 67 (1986).